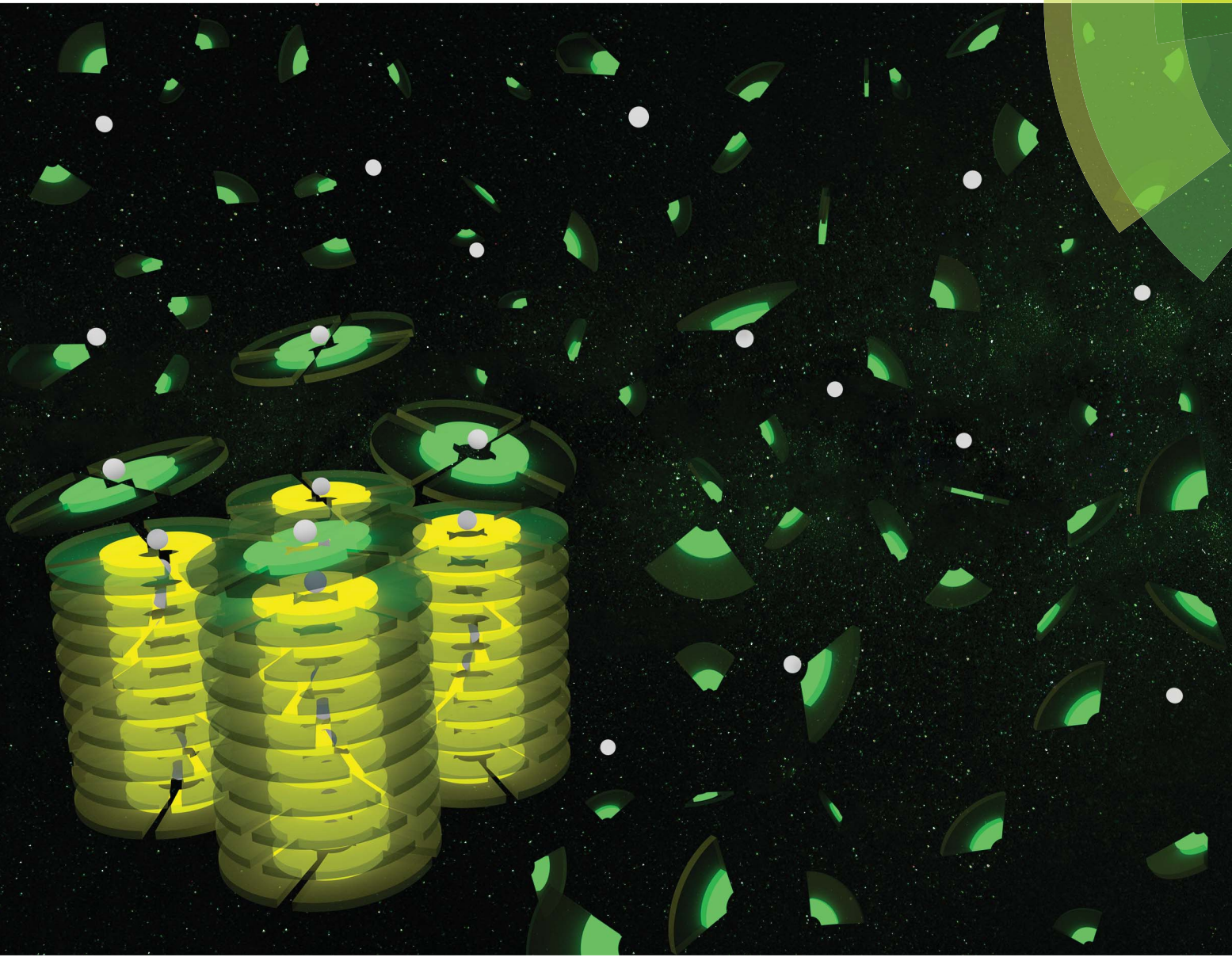


Chemical Science

rsc.li/chemical-science



ISSN 2041-6539



EDGE ARTICLE

Masafumi Yoshio, Takashi Kato *et al.*
Guanine–oligothiophene conjugates: liquid-crystalline
properties, photoconductivities and ion-responsive
emission of their nanoscale assemblies

Cite this: *Chem. Sci.*, 2018, **9**, 576

Guanine–oligothiophene conjugates: liquid-crystalline properties, photoconductivities and ion-responsive emission of their nanoscale assemblies†

Kian Ping Gan, Masafumi Yoshio, ‡* Yuki Sugihara and Takashi Kato *
✉ kato@chiral.t.u-tokyo.ac.jp

We here report the supramolecular self-assembly of hydrogen-bonded motifs for the development of nanostructured materials that exhibit dynamic functions such as stimuli-responsive properties and molecular recognition behaviour. We have designed and synthesised new thermotropic bicontinuous and columnar liquid-crystalline (LC) guanine–oligothiophene conjugates tethered with lipophilic chains, which exhibit ionic, electronic and photoluminescence properties. Their potassium salt complexes self-assemble into thermotropic columnar LC phases. Time-of-flight photoconductivity measurements have revealed that the guanine–oligothiophene conjugates in the LC states possess charge transport abilities with either electron or ambipolar mobility values of 10^{-4} to $10^{-3} \text{ cm}^2 \text{ V}^{-1} \text{ s}^{-1}$. Furthermore, we have found that the complexation of potassium ions with the guanine motif could lead not only to structural change and thermal stabilization of the LC phases but also to a photoluminescence colour change in the solid states. The strategy presented in this work could lead to the design of new functional LC materials that could potentially be applicable as sensors and electronic devices.

Received 28th August 2017
Accepted 24th October 2017DOI: 10.1039/c7sc03764c
rsc.li/chemical-science

Introduction

The use of supramolecular self-assembly of hydrogen-bonded motifs bearing π -conjugated moieties into nanofibers, nano-ribbons, nanocoils, nanorings, liquid crystals, and other self-assembled structures has attracted attention as an emergent approach for the creation of electro- and photo-active advanced materials.^{1–9} The structural complexity and stimuli-responsive nature on the basis of dynamic and directional hydrogen bonds is expected to lead to innovations in their device applications. Amongst them, supramolecular liquid crystals^{2,3,8,10–24} that combine molecular order and fluidity appear to be one of the most promising platforms for exploring memory and sensor materials.^{15,20–23}

Here we report the development of charge-transporting and photoluminescent liquid-crystalline (LC) assemblies based on guanine–oligothiophene conjugates for the first time. Guanine derivatives are a type of hydrogen-bonded self-assembling motif with the versatile ability to form disk-like (Scheme 1a) or ribbon-

like polymorphs (Scheme 1b and c).²⁵ They are able to recognise alkali ions to form guanine tetramers (G-tetrad) which self-assemble to form columnar structures.^{25–33} These properties of guanine derivatives are intriguing for the design of new biomolecule-inspired materials.

We previously reported stimuli-responsive liquid crystals based on folic acid derivatives with a hydrogen-bonding pterin moiety that are structurally similar to guanine,^{34–39} with the main focus on the ion-responsive structural change of liquid crystals and ion-transport properties. However, guanine-based π -conjugated supramolecular liquid crystals for application in organic semiconductors and ion-responsive photoluminescent emitters remain unexplored. In addition, nucleobases such as guanine are also known to exhibit charge carrier transport in deoxyribonucleic acid (DNA) strands.^{40–51} As such, they have also been incorporated as a moiety in other molecules and exploited as semiconductors for various potential applications such as organic photovoltaic devices (OPVs)³¹ and organic field effect transistors (OFETs).⁵²

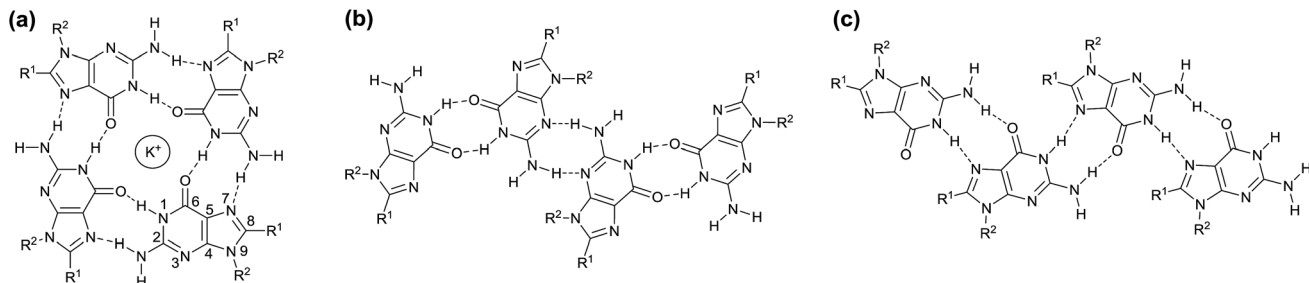
In the present study, we designed a new family of guanine derivatives, **1**, **2a**, **2b**, **3a** and **3b**, containing an *N*-9 alkyl chain and attached *via* wedge-shaped oligothiophenes at the C-8 position (Scheme 2). Oligothiophenes incorporating oligopeptide^{53,54} or nucleobase^{55,56} moieties have previously been explored for their self-assembly properties. Inspired by these studies, we envisioned that the π -conjugation between oligothiophenes and guanine moieties could lead to the induction of liquid crystallinity with a wide temperature range and charge transport properties. The ribbon-like to disk-like structural

Department of Chemistry and Biotechnology, School of Engineering, The University of Tokyo, Hongo, Bunkyo-ku, Tokyo 113-8656, Japan. E-mail: kato@chiral.t.u-tokyo.ac.jp; Fax: +81-3-5841-8661; Tel: +81-3-5841-7440

† Electronic supplementary information (ESI) available: Experimental, gHMBC NMR spectrum, DSC traces, lattice analyses, WAXRD spectra, POM images, FTIR spectra and transient photocurrent curves. See DOI: 10.1039/c7sc03764c

‡ Current address: Semiconductor Nano-interfaces Group, Research Center for Functional Materials, National Institute for Materials Science, Namiki, Tsukuba, Ibaraki 305-0044, Japan, E-mail: yoshio.masafumi@nims.go.jp, Tel: +81-298-60-4728, Fax: +81-298-60-4718.





Scheme 1 (a) Hydrogen-bonded (N1H–O6 and N2H–N7) G-tetrad complexed with a potassium ion, (b) the ribbon-like structure of guanine through the N1H–O6 and N2H–N3 hydrogen bonds, and (c) the ribbon-like structure of guanine through the N1H–N7 and N2H–O6 hydrogen bonds.

change of the guanine moieties could be induced with the introduction of alkali ions, which would alter the fluorescence response of the conjugates. These ion-responsive LC properties and emission colour tuning could lead to potential applications in new sensors and organic light emitting diode (OLED) devices.

Experimental section

Syntheses and characterisation

Five molecules consisting of *N*-9 alkylated guanine conjugated with phenylthiophene (**1**), phenylbithiophene (**2a** and **2b**) or phenylterthiophene (**3a** and **3b**) at the C-8 position of guanine were synthesised (Scheme 3) based on previously reported palladium-catalysed coupling reactions⁵⁷ (ESI, Section 1†). The stereochemistry of *N*-9 alkylated 2-amino-6-benzylxyloxy-9-octylpurine (**9**), a precursor for the guanine–oligothiophene conjugates, was identified by a gHMBC 2D NMR experiment (ESI, Fig. S1†). The bithiophene-based guanine–oligothiophene conjugates were synthesised by a Suzuki–Miyaura cross-coupling reaction of the benzyl-protected *N*-9 alkylated guanine **10** with the *n*-dodecyloxy phenyl bithiophene pinacol esters **7a** and **7b** to afford the corresponding **14a** and **14b**, followed by BCl_3 /pentamethyl benzene cleavage of the benzyl group⁵⁸ to afford the desired guanine–bithiophene derivatives **2a** and **2b**. The mono thiophene- and terthiophene-based derivatives were synthesised using similar procedures. Suzuki–Miyaura coupling reactions of the benzyl-protected guanine **12** with the pinacol esters **6**, **7a** and **7b** afforded **13**, **15a** and **15b**, respectively. Cleavage of the benzyl protecting group afforded the desired guanine–oligothiophene derivatives **1**, **3a** and **3b**. All of the final compounds were recrystallised to remove any residual ions. The molecular structures were

characterised by ^1H and ^{13}C NMR spectroscopy, MALDI-TOF mass spectrometry and elemental analysis.

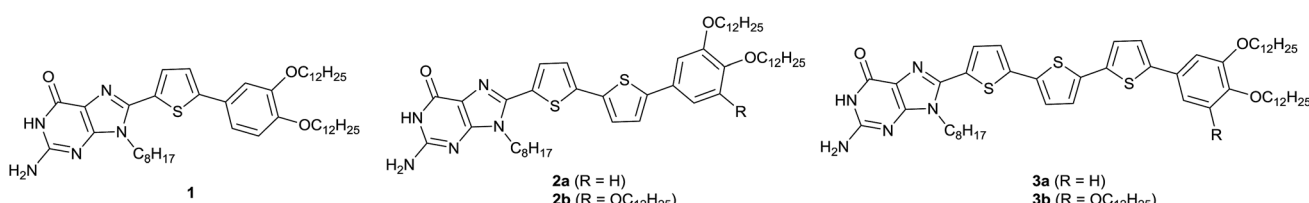
Results and discussion

Liquid-crystalline properties

The thermotropic LC properties and wide-angle X-ray diffraction (WAXRD) data of the guanine–oligothiophene conjugates are summarised in Table 1. The transition temperatures were determined *via* differential scanning calorimetry (DSC) measurements (ESI, Section 3†). Polarising optical microscope (POM) images and WAXRD patterns are shown in Fig. 1 (ESI, Section 4† for lattice analyses of the LC phases).

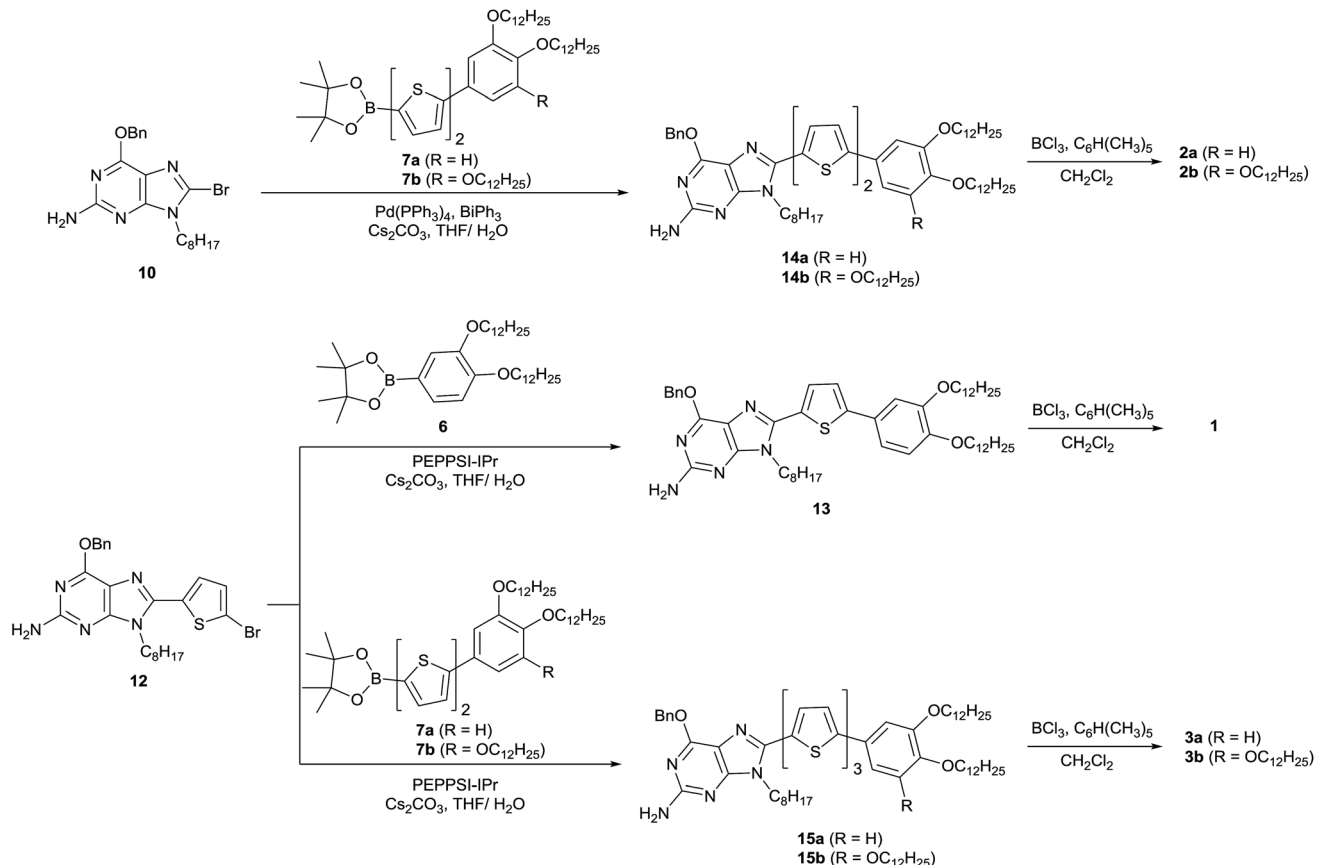
As determined by the DSC thermograms, POM photographs and XRD spectra, compounds **1** and **2a** exhibit no observable mesogenic phase (ESI, Fig. S2a and S3a for the DSC traces, and Fig. S7a and S8a for the WAXRD patterns†). In contrast, the bithiophene-based compound **2b** consisting of a fan-shaped tri(dodecyloxy)phenyl group exhibits a wide range of LC phase from 205 to $-19\text{ }^\circ\text{C}$ upon cooling (ESI, Fig. S4†). Observation under the POM shows the characteristic texture for a columnar phase that is in poly domain alignment between the glass substrates (Fig. 1a). The WAXRD patterns of **2b** at $25\text{ }^\circ\text{C}$ show three diffraction peaks at 41.3 (100) , 25.8 (110) , and 20.0 \AA (200) (Fig. 1b) with a reciprocal *d*-spacing ratio of $1 : \sqrt{3} : 2$, indicating the formation of a one-dimensional nanostructured hexagonal columnar (Col_h) phase. The Col_h structure is presumably stabilised by the stacking of G-tetrads formed through the N1H–O6 and N2H–N7 hydrogen bonds of guanine moieties, as discussed in a later section.

The terthiophene-based compound **3b** containing a fan-shaped tri(dodecyloxy)phenyl group also forms the Col_h phase



Scheme 2 Molecular structures of the guanine–oligothiophene conjugates **1**, **2a**, **2b**, **3a** and **3b**.





Scheme 3 Synthetic schemes of the guanine-oligothiophene conjugates 1, 2a, 2b, 3a and 3b.

in a wide temperature range from 225 to $-13\text{ }^{\circ}\text{C}$ on cooling (ESI, Fig. S6†). The POM observation of **3b** at $25\text{ }^{\circ}\text{C}$ shows a striated fan texture (Fig. 1e), which suggests that the phase possesses more order than that of **2b**. The hexagonal order is clarified by the six-fold diffraction spots in the two-dimensional small-angle XRD (SAXRD) pattern (Fig. 1g), although the WAXRD pattern (Fig. 1f) notes the absence of a (110) peak and shows two peaks at 46.0 (100) and 23.1 \AA (200) with a halo of 4.4 \AA .

In contrast to **3b** with three alkoxy chains the POM image for compound **3a**, having two alkoxy chains, shows no observable birefringence (Fig. 1c). The WAXRD pattern of **3a** at $100\text{ }^{\circ}\text{C}$ reveals diffraction peaks at 46.5 (110) , 29.5 (200) , 23.8 (211) , 17.2 (222) , 15.7 (321) , and 14.6 \AA (400) (Fig. 1d and ESI, Section 4†). As compound **3a** has a lower volume of hydrophobic parts compared to **3b**, these diffraction peaks suggest that **3a** forms a three-dimensional (3D) nanostructured cubic bicontinuous (Cub_{bi}) phase with an *Im3m* lattice, which is quite rare for π -

Table 1 Phase transition thermal properties and XRD data for the guanine-oligothiophene conjugates 1, 2a, 2b, 3a and 3b

Compounds	Phase transition behaviour ^a			XRD data		
	Cooling	Heating		T/°C	Lattice parameters/Å	
1	Iso -30 G	G -28 Iso		—	—	
2a	Iso -16 G	G -12 Iso 118 (-17)	Cr 148 Iso (17)	—	—	
2b	Iso 205 (1)	Col _h -19 Cr (11)	Cr -16 (11)	Col _h 210 Iso (1)	25	47.7
3a	Iso 122 (7)	Cub _{bi} 64 Cr (4)	Cr 65 (4)	Cub _{bi} 143 (-7)	100	58.9
3b	Iso 225 (1)	Col _h -13 Cr (10)	Cr -9 (10)	Col _h 231 Iso (1)	25	53.1

^a Transition temperatures (°C) and transition enthalpies (kJ mol⁻¹) in parentheses, deduced by DSC upon cooling and heating (10 K min⁻¹). Iso, isotropic liquid; G, glassy; Cr and Cr', crystal; Col_h, hexagonal columnar phase; Cub_{bi}, bicontinuous cubic phase.

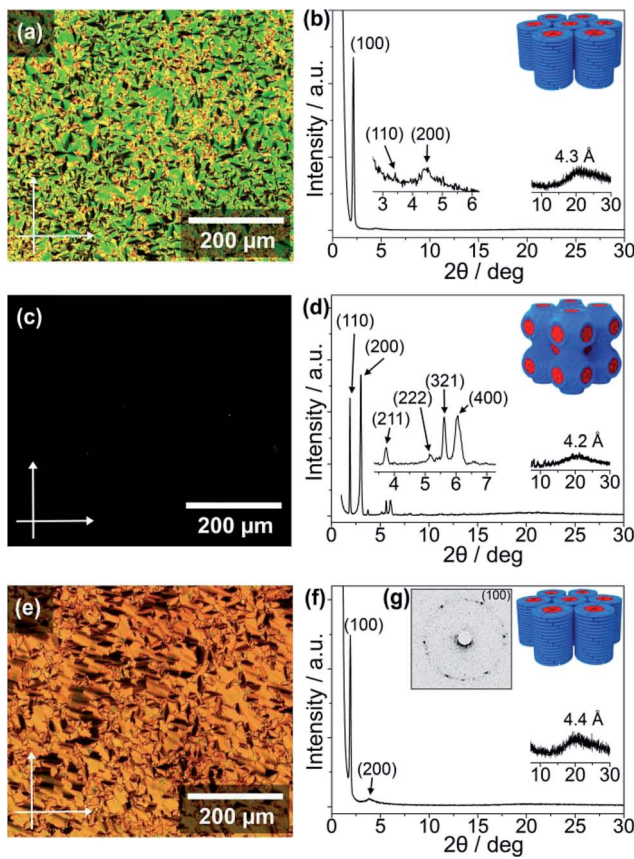


Fig. 1 Polarising optical micrographs with vertical and horizontal arrows indicating the analyser and polariser directions (left panels), and WAXRD spectra with illustrations of the LC nanostructures (right panels): (a and b) compound **2b** in the Col_h phase at 25 °C, (c and d) **3a** in the Cub_{bi} phase ($\text{Im}3\text{m}$ symmetry) at 100 °C, and (e and f) **3b** in the Col_h phase at 25 °C. (g) The 2D small-angle XRD pattern of **3b** at 25 °C. The blue and red parts in the illustrations of the LC nanostructures depict the alkoxyphenyl parts and guanine–oligothiophene mesogenic cores, respectively.

conjugated liquid crystals. The Cub_{bi} phase of **3a** is formed in a wide temperature range from 122 to 64 °C upon cooling (ESI, Fig. S5a†). This unexpected discovery of the Cub_{bi} LC phase will open up new opportunities for charge carrier transport and photoluminescent materials.

Charge carrier transport

As mentioned earlier, guanine and other nucleobases are nature's semiconductors. In this regard, conjugation between guanine and oligothiophenes could create materials that could potentially be applied as organic semiconductors. Therefore, the hole and electron charge carrier transport properties of the LC compounds **2b**, **3a** and **3b** were examined using the time-of-flight (TOF) photoconductivity method. The LC samples were sandwiched in ITO cells and a potential bias was applied through the cell, followed by charge carrier generation by excitation from a laser pulse source. The charge carrier mobility values derived from the transient photocurrent curves (ESI,

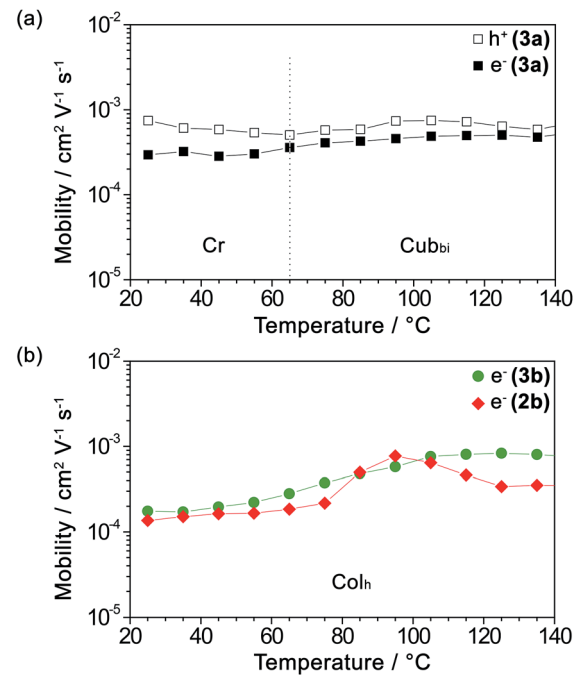


Fig. 2 Logarithmic plots of (a) the hole mobility (\square) and electron mobility (\blacksquare) of **3a** and (b) the electron mobility of **3b** (\bullet) and **2b** (\blacklozenge) as a function of temperature upon heating.

Fig. S10†) are plotted as a function of temperature in Fig. 2a for **3a** and Fig. 2b for **2b** and **3b**.

We found that compound **3a** exhibits ambipolar charge carrier transport properties with hole and electron mobility values in the order of 10^{-4} to $10^{-3} \text{ cm}^2 \text{V}^{-1} \text{s}^{-1}$ in the Cub_{bi} phase and the Cr phase as well (Fig. 2a and ESI, Fig. S10a–c†), with the values of hole mobility slightly higher than those of the electron mobilities. In contrast, compounds **2b** and **3b** in their Col_h phases possess only electron transport properties with electron mobility values of 10^{-4} to $10^{-3} \text{ cm}^2 \text{V}^{-1} \text{s}^{-1}$ (Fig. 2b and ESI, Fig. S10d–f†). The electron mobility of **3b** increases with an increase in temperature. As for **2b**, which has a shorter π -conjugation length, the electron mobility value reaches a maximum at 95 °C, possibly due to the formation of an optimal π -stacked molecular arrangement during the viscosity change upon heating.

On the other hand, the transient photocurrents of **2b** and **3b** obtained by applying a positive bias exhibit weak and dispersive signals, which is probably attributed to the hole trapping effect. It has been previously reported that guanine–guanine stacks in DNA strands serve as shallow hole traps,^{42–44,50} which have the effect of causing highly dispersive photocurrent curves for holes and dramatically decreasing the hole carrier transport.⁵⁹

Molecular modelling study

In order to make sense of the carrier transport properties of the guanine–oligothiophene conjugates, the frontier molecular orbitals of the guanine–bithiophene conjugate **2b** and guanine–terthiophene conjugate **3a** were determined computationally (Fig. 3) using density functional theory (DFT).

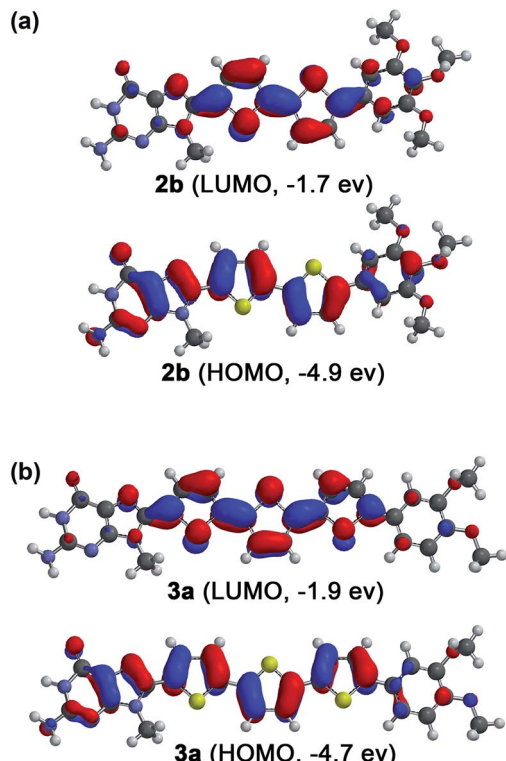


Fig. 3 Computationally calculated HOMOs and LUMOs of phenyl-methoxy- and *N*-9 methyl-substituted model compounds (a) for **2b** and (b) for **3a** by the DFT method with B3LYP/6-31G(d) parameters.

The HOMOs for both molecules consist of contributions from both the oligothiophene and guanine moieties, while for the LUMOs the guanine moiety has minimal contribution. This implies that if it is supposed that the π - π stacking is guanine dominant, such as in the case of a tetrameric stacking structure, hole transport properties may be expected. However, as discussed previously, this stacking of guanines can lead to a detrimental effect on the hole carrier transport properties. In contrast, stacking of the oligothiophenes should lead to electron transport properties.

As previously revealed by the TOF photoconductivity measurements, compound **3a** exhibits ambipolar charge carrier transport, which can be explained by two factors: (1) the Cub_{bi} phase allows three-dimensional transport for both holes and electrons without the need for alignment in the sandwiched ITO cells, and (2) guanine-guanine (G-G) stacking is limited in the Cub_{bi} assembly, which can help to avoid the shallow hole traps found in the G-G stacks. In this regard, compounds **2b** and **3b** in the Col_h phases are (1) polydomain with respect to the ITO substrates, and (2) tetrameric with stacked guanines in the LC assembly that could potentially lead to shallow hole traps.⁵⁰ These two factors for both **2b** and **3b** possibly lead to inhibition of the hole transport properties in the columnar structures, allowing only electron carrier transport.

Potassium ion-induced LC properties

As guanine derivatives tend to form 8 : 1 or 4 : 1 complexes with respect to potassium ions,²⁸ these organic to K^+ ratios were used

to investigate the ion-responsive liquid crystallinity of compounds **1**, **2a** and **3a** when potassium trifluoromethanesulfonate ($\text{CF}_3\text{SO}_3\text{K}$) was introduced. $\text{CF}_3\text{SO}_3\text{K}$ was selected as the potassium source due to the excellent thermal stability of the trifluoromethanesulfonate anion. The phase transition temperatures of the respective guanine-oligothiophene liquid crystals and their complexes with K^+ were characterised *via* DSC and WAXRD (ESI, Section 3 for the DSC thermograms and Section 5 for the WAXRD spectra of the liquid crystal: K^+ complexes†) and are summarised in Fig. 4.

While both compounds **1** and **2a** exhibit no LC phases in their single-component states, the introduction of K^+ induces the formation of columnar phases for both of the compounds at room temperature. The 8 : 1 molar complex of **1** with $\text{CF}_3\text{SO}_3\text{K}$ shows an ordered hexagonal columnar (Col_{ho}) phase from 244 to -22 °C upon cooling (Fig. 4a), with a typical fan-shaped texture when observed under the POM (ESI, Fig. S11a†). The introduction of excess $\text{CF}_3\text{SO}_3\text{K}$ causes no significant change in the glass transition temperature, while another disordered hexagonal columnar phase (Col_{hd}) at above 113 °C upon cooling is observed for the 2 : 1 molar complex.

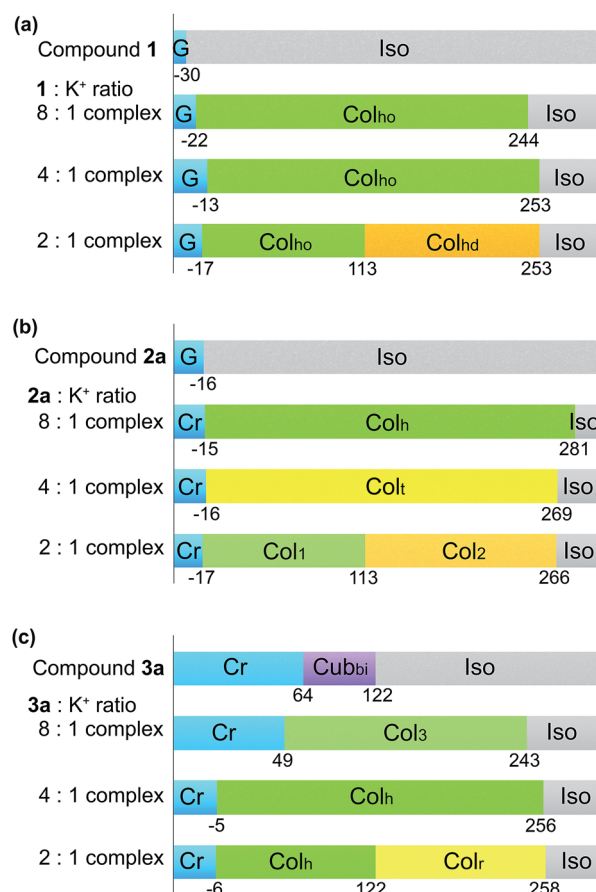


Fig. 4 Phase transition temperatures (°C) of the guanine derivatives and their complexes with $\text{CF}_3\text{SO}_3\text{K}$ at different molar ratios: (a) for **1**, (b) for **2a** and (c) for **3a**. The temperatures were deduced from the DSC traces upon first cooling (10 K min^{-1}). Col_{ho} , ordered hexagonal columnar phase; Col_{hd} , disordered hexagonal columnar phase; Col_t , tetragonal columnar phase; Col_r , rectangular columnar phase; Col_1 , Col_2 and Col_3 , columnar phases with undefined geometries.



The 8 : 1 molar complex of **2a** with $\text{CF}_3\text{SO}_3\text{K}$ also exhibits a wide temperature range of the Col_h phase from 281 to -15°C (Fig. 4b), with a typical texture for the columnar phase under POM observation (ESI, Fig. S11f†). A tetragonal columnar (Col_t) phase and two unidentified columnar phases (Col_1 , Col_2) were induced with 4 : 1 and 2 : 1 molar complexes of **2a** : $\text{CF}_3\text{SO}_3\text{K}$.

On the other hand, the introduction of K^+ to compound **3a** to form the Cub_{bi} phase led to the induction of columnar phases with a significant increase in the isotropic temperature (Fig. 4c). As the K^+ to **3a** molar ratio increases, unidentified columnar (Col_3), Col_h and rectangular columnar (Col_r) phases are observed. The Col_3 phase is hypothesised to be an intermediate phase between the Cub_{bi} and Col_h phases. The crystallisation temperature of the complexes shows a decreasing trend with the increase of K^+ in the complexes. The properties of these ion-responsive liquid crystals will be explored in a later section.

While it has been considered that the change in the LC assemblies induced by the introduction of K^+ could have an effect on the charge carrier transport, the photoconductivity measurements of the complexes are excluded from our current study due to the difficulty in the preparation of measurement cells containing the complexes with very high clearing points.

FTIR spectroscopic studies

As a means to gain an insight into the hydrogen bonding structures of the guanine–oligothiophene conjugates, all of the guanine–oligothiophene derivatives and their complexes with $\text{CF}_3\text{SO}_3\text{K}$ were characterised *via* Fourier transform infrared (FTIR) spectroscopy (Fig. 5 and ESI, Fig. S12†).

Guanine–bithiophene derivatives **2a** and **2b** in the isotropic and Col_h phases, respectively, at room temperature show almost identical spectra (Fig. 5a). For compound **2a** with a di(dodecyloxy)phenyl moiety, the amine N_2H asymmetric stretch band $\nu_a(\text{N}_2\text{H})$ at 3306 cm^{-1} , the symmetric N_2H stretch bands $\nu_s(\text{N}_2\text{H})$ at 3205 , 3154 and 3070 cm^{-1} , and two carbonyl stretch bands $\nu(\text{C=O})$ at 1681 and 1676 cm^{-1} from the guanine moiety can be observed (Fig. 5a).⁶⁰ As for compound **2b**, which has a fan-shaped tri(dodecyloxy) moiety, only one carbonyl peak at $\nu(\text{C=O})$ at 1681 cm^{-1} can be seen.

Compound **2a** complexed with $\text{CF}_3\text{SO}_3\text{K}$ also shows one carbonyl peak at $\nu(\text{C=O})$ at 1688 cm^{-1} in its FTIR spectrum. The 8 : 1 molar complex of compound **2a** with $\text{CF}_3\text{SO}_3\text{K}$ exhibits redshifts in two of the amine peaks, $\nu_a(\text{N}_2\text{H})$ at 3288 cm^{-1} and $\nu_s(\text{N}_2\text{H})$ at 3112 cm^{-1} . The redshifts of the amine peaks could be attributed to the ion–dipole interactions of the alkali ion on the G-tetrads, resulting in weaker N–H bonds. Similar observations can be made for the FTIR spectra of compound **1** and its potassium salt complex (ESI, Fig. S12†).

Guanine–terthiophene derivatives exhibit similar FTIR spectra to their guanine–bithiophene counterparts. Compound **3a** shows $\nu_a(\text{N}_2\text{H})$ at 3316 cm^{-1} , $\nu_s(\text{N}_2\text{H})$ at 3206 , 3147 and 3066 cm^{-1} and $\nu(\text{C=O})$ at 1682 and 1671 cm^{-1} , and the detection of the two distinct carbonyl peaks is exclusive to the di(dodecyloxy) moiety attached guanine–terthiophene derivative **3a** (Fig. 5b). Similarly, a shift to a lower wavenumber of the

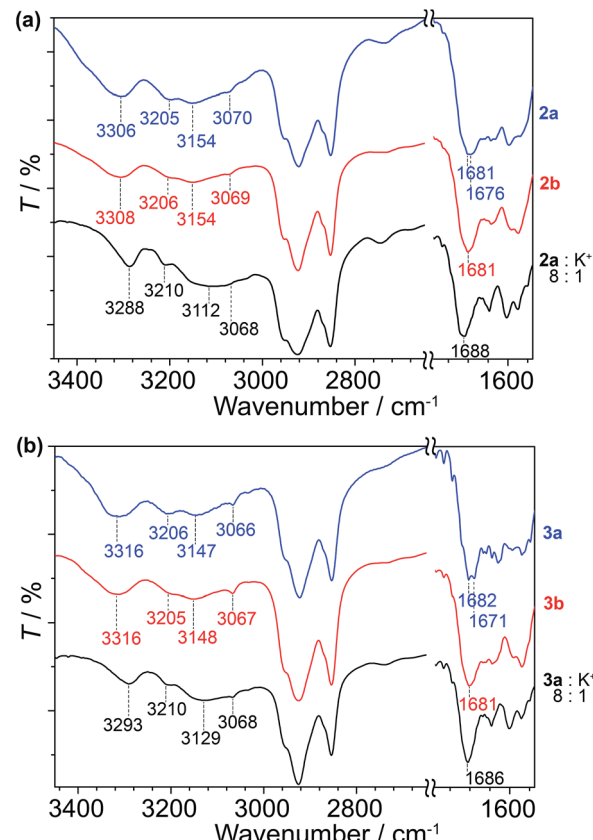


Fig. 5 FTIR spectra of (a) **2a**, **2b** and the complex of **2a** with $\text{CF}_3\text{SO}_3\text{K}$ at room temperature and (b) **3a**, **3b** and the complex of **3a** with $\text{CF}_3\text{SO}_3\text{K}$ at 100°C .

amine peaks is observed for the 8 : 1 molar complex of compound **3a** with $\text{CF}_3\text{SO}_3\text{K}$.

The observed two $\nu(\text{C=O})$ stretching bands for compounds **1** and **2a** in the Iso phases and **3a** in the Cub_{bi} phase can be ascribed to $\nu(\text{C=O})$ coupled with the NH_2 scissoring and N_1H in-plane bending vibrations.⁶⁰ Whereas for the Col_h phases of the fan-shaped **2b**, **3b**, and various guanine–oligothiophene complexes with K^+ , the single $\nu(\text{C=O})$ peak suggests that the adoption of a single configuration of the hydrogen bonding through $\text{N}_1\text{H–O}_6$ and $\text{N}_2\text{H–N}_7$ (G-tetrads) of the guanine moiety eliminates such a coupling effect. As such, through these experimental observations, we proposed that more than one configuration of hydrogen bonding structures is present for the Iso and Cub_{bi} phases of compounds **1**, **2a** and **3a** (*vide infra*).

Proposed self-assembled structures

Based on the XRD data, FTIR, charge transport properties and molecular modelling studies, the self-assembled structures of the guanine–oligothiophene derivatives are proposed.

The number of formula units per unit cell (Z) for compound **3a** was calculated to be approximately 8 (ESI, Section 4†). Hence, it is proposed that compound **3a** in the Cub_{bi} phase self-assembled in a ribbon-like, catenary-like form (Fig. 6a). Similar molecular arrangements have previously been



reported.³⁰ In this case, N1H–O6, N2H–O6 and N2H–N3 hydrogen bonds are present in the nanoscale assembly. Moreover, this molecular assembly is supposedly arranged in such a way that guanine–guanine stackings are non-dominant, reducing hole traps and allowing ambipolar transport in the nanostructures. The molecular assembly of the eight molecules of **3a** measures 72 by 76 Å, which is larger than the lattice parameter derived from the WAXRD spectra at 58.9 Å. It is proposed that the alkyl chains fit into the space between adjacent oligothiophene groups, resulting in a smaller-than-simulated lattice parameter.

Compound **3b** is proposed to form G-tetrads that stack on top of each other to form a columnar structure (Fig. 6b). The column diameter for compound **3b** was calculated to be approximately 61 Å. This theoretical column diameter is observably longer than the diameter of the column as determined by the WAXRD patterns at 53.1 Å, which can be explained by interdigitating of the alkyl chains as well. Compound **2b** is also thought to share a similar self-assembled structure.

Ion-stimuli responsive emission properties

The UV-vis absorption and emission response of the ion-responsive liquid crystals were investigated *via* UV-vis absorption and fluorescence spectroscopy (Fig. 7) and by visual inspection under the illumination of UV light (Fig. 8).

The absorption spectrum of **1** shows a plateau with a peak at 380 nm, with a drop off at 420 nm, while all of the complexes of **1** with $\text{CF}_3\text{SO}_3\text{K}$ exhibit a distinct peak at 360 nm which can be

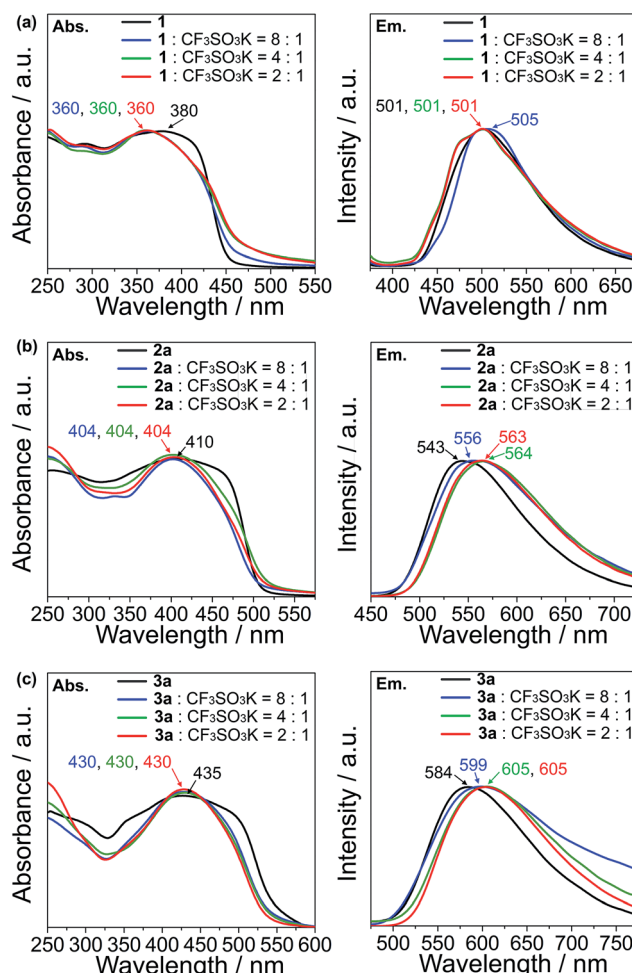


Fig. 7 Normalized UV-vis absorbance (left panels) and emission (right panels) spectra of (a) **1** and its K^+ complexes, (b) **2a** and its K^+ complexes and (c) **3a** and its K^+ complexes. The excitation wavelengths of **1**, **2a** and **3a** are 365, 410 and 430 nm, respectively.

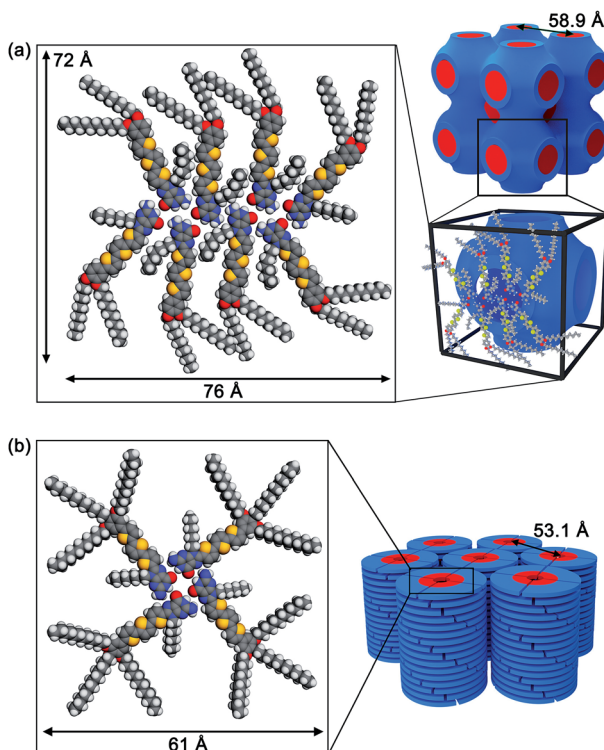


Fig. 6 Proposed molecular assembled structures of (a) **3a** in the Cub_{bi} phase and (b) **3b** in the Col_{h} phase.

ascribed to the $\pi \rightarrow \pi^*$ transition (Fig. 7a, left). As for the emission spectra, there are no appreciable shifts in the emission wavelength for compound **1** and its K^+ complexes, with an emission peak at 501 nm which corresponds to the $\text{S}_1 \rightarrow \text{S}_0$ relaxation (Fig. 7a, right).

Compound **2a** exhibits an absorption peak that shows a plateau until 470 nm with a maximum at 410 nm ($\pi \rightarrow \pi^*$), while its complexes exhibit a more distinct peak at 404 nm (Fig. 7b, left). On the other hand, the emission peaks exhibit a redshift that increases in magnitude as the K^+ ratio increases in the complexes, from 543 nm ($\text{S}_1 \rightarrow \text{S}_0$) for compound **2a**, to 556 nm for the 8 : 1 molar complex of **2a** with $\text{CF}_3\text{SO}_3\text{K}$ (Fig. 7b, right). The redshift is maximised with 4 : 1 and 2 : 1 molar complexes at 564 and 563 nm, respectively.

Compound **3a** and its complexes show a similar trend. **3a** shows a less distinct absorption peak at 435 nm ($\pi \rightarrow \pi^*$) with a plateau that ends at 490 nm, while its K^+ complexes exhibit a distinct peak at 430 nm (Fig. 7c, left). Similar to the emission spectra of compound **2a**, the addition of K^+ to compound **3a** induces a redshift in the spectra. While **3a** shows an emission



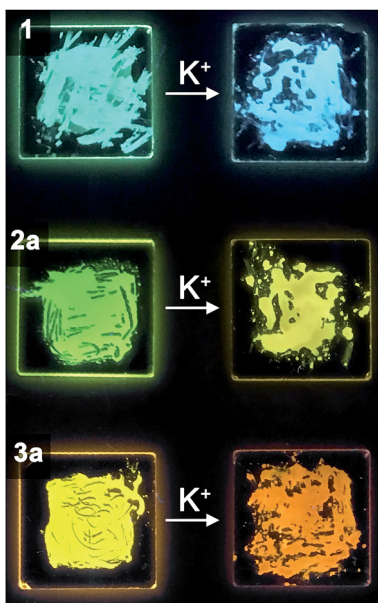


Fig. 8 Photographs of the guanine–thiophene conjugate 1, guanine–bithiophene conjugate 2a and guanine–terthiophene conjugate 3a (left panels) and their respective 4 : 1 molar complexes with $\text{CF}_3\text{SO}_3\text{K}$ (right panels) at room temperature on quartz plates under the illumination of UV light (365 nm).

peak at 584 nm ($\text{S}_1 \rightarrow \text{S}_0$), the 8 : 1 molar complex of 3a with the $\text{CF}_3\text{SO}_3\text{K}$ complex exhibits a peak at 599 nm, and at 605 nm for both the 4 : 1 and 2 : 1 molar complexes (Fig. 7c, right).

The observation of distinct peaks in the UV-vis absorption spectra for the K^+ complexes instead of plateaus, as seen for uncomplexed guanine–oligothiophene conjugates, can be explained by the formation of discrete nanoscale assembly in the columnar phases that limits the possible excitation pathways. As for the emission spectra, compound 1 exhibits no significant bathochromic shift probably due to insufficient overlapping from the monothiophene moiety. On the contrary, the bathochromic shifts for the emission peaks for compounds 2a and 3a with K^+ can be attributed to the increased π – π stacking interactions of the columnar phases. The stacking distance is thought to further decrease with respect to the increase in K^+ ions, with the interactions between each layer maximised with the 4 : 1 complexes.

For compounds 2b and 3b in the Col_h phases, the introduction of K^+ also causes a redshift (ESI, Section 9†), but with a magnitude of change less significant than that of the K^+ complexes of 2a and 3a.

In order to gain further insight into the emission colour change in the bulk states, we conducted studies of the absorbance and emission spectra of the THF solution of guanine–oligothiophene conjugates in the presence of K^+ ions (ESI, Fig S15†). It has been previously reported that G-tetrads are formed in THF solution with a concentration of 10^{-3} M or higher, while the monomeric form exists at a concentration of 10^{-4} M or lower.^{30–33} As such, THF solutions containing guanine–oligothiophenes conjugates with a concentration of 2×10^{-5} M

(Fig. S15a†) and 4×10^{-3} M (Fig. S15b†) in the presence of $\text{CF}_3\text{SO}_3\text{K}$ (3.6×10^{-3} M) were prepared and characterised *via* UV-vis absorption and fluorescence spectroscopy.

Through our investigation, it was discovered that the presence of high concentrations of K^+ does not affect the spectra of dilute solutions (2×10^{-5} M) in any noticeable way. On the other hand, the concentrated solutions (4×10^{-3} M) exhibited observable spectroscopic redshift in the emission spectra when K^+ was introduced, indicating the formation of G-tetrads and subsequently better π – π stacking interactions resulting from such a molecular assembly. Thus, we believe that the colour change when K^+ is introduced to guanine–oligothiophene conjugates is a result of increased molecular stacking induced by ion–dipole interactions.

Conclusion

We have demonstrated that the LC properties and photonic behaviour of hydrogen-bonded π -conjugates can be tuned through complexation and binding of potassium ions. We have also established that guanine–oligothiophene conjugates adopt nanoscale assembly structures that exhibit charge transport properties. This is a new approach in the field of supramolecular materials, where ionic, photonic, and electronic functions are induced in the same molecule. The presented strategy would contribute to the development of materials in organic electronics and sensor devices.

Conflicts of interest

There are no conflicts to declare.

Acknowledgements

This study was partially supported by Scientific Research on Innovative Areas (Stimuli-responsive Chemical species, KAKENHI 15H00921 for M. Y.) from the Ministry of Education, Culture, Sports, Science and Technology of Japan (MEXT). This work was also partially supported by CREST, JST (JPMJCR1422) for T. K. K. P. G. is grateful for the support of MEXT for his research and pursuit of graduate degrees at the University of Tokyo.

Notes and references

- 1 *Supramolecular Soft Matter: Applications in Materials and Organic Electronics*, ed. T. Nakanishi, John Wiley & Sons, Hoboken, NJ, 2011.
- 2 T. Kato, N. Mizoshita and K. Kishimoto, *Angew. Chem., Int. Ed.*, 2006, **45**, 38–68.
- 3 S. J. Rowan and P. T. Mather, in *Liquid Crystalline Functional Assemblies and Their Supramolecular Structures, Structure and Bonding*, ed. T. Kato, Springer Berlin Heidelberg, Berlin, Heidelberg, 2008, vol. 128, pp. 119–149.
- 4 S. Yagai and A. Kitamura, *Chem. Soc. Rev.*, 2008, **37**, 1520–1529.

5 C. C. Lee, C. Grenier, E. W. Meijer and A. P. H. J. Schenning, *Chem. Soc. Rev.*, 2009, **38**, 671–683.

6 L. E. Buerkle and S. J. Rowan, *Chem. Soc. Rev.*, 2012, **41**, 6089–6102.

7 S. S. Babu, V. K. Praveen and A. Ajayaghosh, *Chem. Rev.*, 2014, **114**, 1973–2129.

8 T. Kato, M. Yoshio, T. Ichikawa, B. Soberats, H. Ohno and M. Funahashi, *Nat. Rev. Mater.*, 2017, **2**, 17001.

9 M. Kumar and S. Kumar, *Polym. J.*, 2017, **49**, 85–111.

10 T. Kato, in *Molecular Self-Assembly Organic Versus Inorganic Approaches, Structure and Bonding*, ed. M. Fujita, Springer Berlin Heidelberg, Berlin, Heidelberg, 2000, vol. 96, pp. 95–146.

11 T. Kato, N. Mizoshita and K. Kanie, *Macromol. Rapid Commun.*, 2001, **22**, 797–814.

12 F. J. M. Hoeben, P. Jonkheijm, E. W. Meijer and A. P. H. J. Schenning, *Chem. Rev.*, 2005, **105**, 1491–1546.

13 B. Donnio, S. Buathong, I. Bury and D. Guillon, *Chem. Soc. Rev.*, 2007, **36**, 1495–1513.

14 C. Tschierske, *Chem. Soc. Rev.*, 2007, **36**, 1930–1970.

15 Z. Chi, X. Zhang, B. Xu, X. Zhou, C. Ma, Y. Zhang, S. Liu and J. Xu, *Chem. Soc. Rev.*, 2012, **41**, 3878–3896.

16 *Handbook of Liquid Crystals*, ed. J. W. Goodby, P. J. Collings, T. Kato, C. Tschierske, H. Gleeson and P. Raynes, Wiley-VCH, Weinheim, Germany, 2nd edn, 2014.

17 T. Kato and J. M. J. Fréchet, *Macromolecules*, 1989, **22**, 3818–3819.

18 T. Kato and J. M. J. Fréchet, *J. Am. Chem. Soc.*, 1989, **111**, 8533–8534.

19 M. Suárez, J.-M. Lehn, S. C. Zimmerman, A. Skoulios and B. Heinrich, *J. Am. Chem. Soc.*, 1998, **120**, 9526–9532.

20 Y. Sagara and T. Kato, *Angew. Chem., Int. Ed.*, 2008, **47**, 5175–5178.

21 Y. Sagara and T. Kato, *Nat. Chem.*, 2009, **1**, 605–610.

22 M. Lehmann, S. Gloza and S. Roth, *Chem. Mater.*, 2015, **27**, 8181–8184.

23 M. Mitani, S. Ogata, S. Yamane, M. Yoshio, M. Hasegawa and T. Kato, *J. Mater. Chem. C*, 2016, **4**, 2752–2760.

24 S. Herbst, B. Soberats, P. Leowanawat, M. Lehmann and F. Würthner, *Angew. Chem., Int. Ed.*, 2017, **56**, 2162–2165.

25 J. T. Davis and G. P. Spada, *Chem. Soc. Rev.*, 2007, **36**, 296–313.

26 S. Sivakova and S. J. Rowan, *Chem. Soc. Rev.*, 2005, **34**, 9–21.

27 S. Zhang, Y. Wu and W. Zhang, *ChemMedChem*, 2014, **9**, 899–911.

28 E. Mezzina, P. Mariani, R. Itri, S. Masiero, S. Pieraccini, G. P. Spada, F. Spinozzi, J. T. Davis and G. Gottarelli, *Chem.-Eur. J.*, 2001, **7**, 388–395.

29 A. Ghoussoub and J.-M. Lehn, *Chem. Commun.*, 2005, 5763–5765.

30 D. González-Rodríguez, P. G. A. Janssen, R. Martín-Rapún, I. D. Cat, S. D. Feyter, A. P. H. J. Schenning and E. W. Meijer, *J. Am. Chem. Soc.*, 2010, **132**, 4710–4719.

31 Y.-L. Wu, K. E. Brown and M. R. Wasielewski, *J. Am. Chem. Soc.*, 2013, **135**, 13322–13325.

32 Y.-L. Wu, K. E. Brown, D. M. Gardner, S. M. Dyar and M. R. Wasielewski, *J. Am. Chem. Soc.*, 2015, **137**, 3981–3990.

33 M. Garcia-Iglesias, T. Torres and D. Gonzalez-Rodriguez, *Chem. Commun.*, 2016, **52**, 9446–9449.

34 T. Kato and N. Mizoshita, *Curr. Opin. Solid State Mater. Sci.*, 2002, **6**, 579–587.

35 T. Kato, T. Yasuda, Y. Kamikawa and M. Yoshio, *Chem. Commun.*, 2009, 729–739.

36 K. Kanie, T. Yasuda, M. Nishii, S. Ujiie and T. Kato, *Chem. Lett.*, 2001, **30**, 480–481.

37 K. Kanie, M. Nishii, T. Yasuda, T. Taki, S. Ujiie and T. Kato, *J. Mater. Chem.*, 2001, **11**, 2875–2886.

38 T. Kato, T. Matsuoka, M. Nishii, Y. Kamikawa, K. Kanie, T. Nishimura, E. Yashima and S. Ujiie, *Angew. Chem., Int. Ed.*, 2004, **43**, 1969–1972.

39 N. Sakai, Y. Kamikawa, M. Nishii, T. Matsuoka, T. Kato and S. Matile, *J. Am. Chem. Soc.*, 2006, **128**, 2218–2219.

40 C. R. Treadway, M. G. Hill and J. K. Barton, *Chem. Phys.*, 2002, **281**, 409–428.

41 H.-A. Wagenknecht, *Nat. Prod. Rep.*, 2006, **23**, 973–1006.

42 J. C. Genereux and J. K. Barton, *Chem. Rev.*, 2010, **110**, 1642–1662.

43 F. D. Lewis, T. Wu, X. Liu, R. L. Letsinger, S. R. Greenfield, S. E. Miller and M. R. Wasielewski, *J. Am. Chem. Soc.*, 2000, **122**, 2889–2902.

44 F. D. Lewis, X. Liu, J. Liu, S. E. Miller, R. T. Hayes and M. R. Wasielewski, *Nature*, 2000, **406**, 51–53.

45 E. M. Conwell and S. M. Bloch, *J. Phys. Chem. B*, 2006, **110**, 5801–5806.

46 F. Ortmann, K. Hannewald and F. Bechstedt, *J. Phys. Chem. B*, 2009, **113**, 7367–7371.

47 F. F. Maia, V. N. Freire, E. W. S. Caetano, D. L. Azevedo, F. A. M. Sales and E. L. Albuquerque, *J. Chem. Phys.*, 2011, **134**, 175101.

48 J. D. Slinker, N. B. Muren, S. E. Renfrew and J. K. Barton, *Nat. Chem.*, 2011, **3**, 228–233.

49 A. K. Thazhathveetil, A. Trifonov, M. R. Wasielewski and F. D. Lewis, *J. Am. Chem. Soc.*, 2011, **133**, 11485–11487.

50 J. Choi, J. Park, A. Tanaka, M. J. Park, Y. J. Jang, M. Fujitsuka, S. K. Kim and T. Majima, *Angew. Chem., Int. Ed.*, 2013, **52**, 1134–1138.

51 L. Xiang, J. L. Palma, C. Bruot, V. Mujica, M. A. Ratner and N. Tao, *Nat. Chem.*, 2015, **7**, 221–226.

52 G. Maruccio, P. Visconti, V. Arima, S. D'Amico, A. Biasco, E. D'Amone, R. Cingolani, R. Rinaldi, S. Masiero, T. Giorgi and G. Gottarelli, *Nano Lett.*, 2003, **3**, 479–483.

53 A. K. Shaytan, E.-K. Schillinger, E. Mena-Osteritz, S. Schmid, P. G. Khalatur, P. Bäuerle and A. R. Khokhlov, *Beilstein J. Nanotechnol.*, 2011, **2**, 525–544.

54 D. A. Stone, A. S. Tayi, J. E. Goldberger, L. C. Palmer and S. I. Stupp, *Chem. Commun.*, 2011, **47**, 5702–5704.

55 G. P. Spada, S. Lena, S. Masiero, S. Pieraccini, M. Surin and P. Samori, *Adv. Mater.*, 2008, **20**, 2433–2438.

56 H. Ouchi, X. Lin, T. Kizaki, D. D. Prabhu, F. Silly, T. Kajitani, T. Fukushima, K.-i. Nakayama and S. Yagai, *Chem. Commun.*, 2016, **52**, 7874–7877.



57 R. Bou Zerdan, P. Cohn, E. Puodziukynaite, M. B. Baker, M. Voisin, C. Sarun and R. K. Castellano, *J. Org. Chem.*, 2015, **80**, 1828–1840.

58 K. Okano, K.-i. Okuyama, T. Fukuyama and H. Tokuyama, *Synlett*, 2008, 1977–1980.

59 C. Li, L. Duan, H. Li and Y. Qiu, *J. Phys. Chem. C*, 2014, **118**, 10651–10660.

60 R. P. Lopes, M. P. M. Marques, R. Valero, J. Tomkinson and L. A. E. B. de Carvalho, *Spectrosc. Int. J.*, 2012, **27**, 20.

